Hydrogen Bonding to the Bound Dioxygen in Oxy Cobaltous Myoglobin Reduces the Superhyperfine Coupling to the Proximal Histidine†

H. Caroline Lee,*,‡ Masao Ikeda-Saito,§ Takashi Yonetani,∥ Richard S. Magliozzo,‡ and Jack Peisach‡,⊥

Department of Molecular Pharmacology and Department of Physiology and Biophysics, Albert Einstein College of Medicine of Yeshiva University, Bronx, New York 10461, Department of Physiology and Biophysics, Case Western Reserve University School of Medicine, Cleveland, Ohio 44106-4970, and Department of Biochemistry and Biophysics, University of Pennsylvania School of Medicine, Philadelphia, Pennsylvania 19104

Received February 28, 1992; Revised Manuscript Received April 24, 1992

ABSTRACT: Electron spin echo envelope modulation (ESEEM) spectroscopy was used to study the electron–nuclear coupling in two oxygenated cobalt-substituted hemoproteins, myoglobin (oxyCoMb) and a monomeric hemoglobin from *Glycera dibranchiata* (oxyCoHb*gly*). The modulation frequency components in ESEEM spectra of both proteins arose from the coupling to the N_ϵ of the proximal histidyl imidazole. The hyperfine and quadrupole coupling parameters for these two nitrogens, calculated by computer spectral simulation, are A_{iso} = 2.46 MHz, e^2qQ = 2.15 MHz, and η = 0.4 for oxyCoMb and A_{iso} = 3.70 MHz, e^2qQ = 2.70 MHz, and η = 0.5 for oxyCoHb*gly*. A hyperfine coupling of 0.6 MHz, found for oxyCoMb in D_2O but not for oxyCoHb*gly* in D_2O, was assigned to the coupling to a deuteron that is hydrogen-bonded to the O_2 ligand in oxyCoMb. This hydrogen bonding is believed to be responsible for the reduction in hyperfine and nuclear quadrupole coupling to the proximal histidyl imidazole N_ϵ in oxyCoMb. A molecular orbital model for O_2 adducts of cobaltous compounds [Tovrog et al. (1976) *J. Am. Chem. Soc. 98*, 5144] was used to understand the hydrogen bond-induced reduction in ^{14}N superhyperfine coupling in oxyCoMb.

The binding of exogenous ligands to the sixth coordination position of the heme iron is related to a variety of functional properties of hemoproteins. Interactions with the protein moiety, for example, through hydrogen bonding, are important factors in governing the binding of the sixth heme ligands. In oxymyoglobin (Mb),[1] the hydrogen bond between the terminal oxygen and the N_ϵ-bound proton on the imidazole of histidine E7 (His-E7)[2] (Phillips & Schoenborn, 1981), the distal histidine, is believed to be an important factor in controlling oxygen affinity. The interaction of the sixth ligand of the heme iron with His-E7 has been extensively studied by comparing Mb to engineered E7 mutants (Nagai et al., 1987; Olson et al., 1988) and monomeric globins lacking the distal histidine (Mims et al., 1983). An important issue not specifically addressed in these studies is how the hydrogen bond affects the interaction of the heme iron with its endogenous axial ligands.

The electron paramagnetic resonance (EPR) spectra of paramagnetic forms of Mb can provide useful information on metal–ligand interactions. Native oxyMb, however, contains a diamagnetic iron center and cannot be investigated by EPR techniques. In contrast, cobalt-substituted Mb (CoMb), in both its deoxy and oxy states, is a functional and EPR-active analogue of the ferrous protein (Hoffman & Petering, 1970). The continuous wave (CW) EPR spectrum of oxyCoMb is of a free radical type centered around $g \approx 2$ (Hoffman & Petering, 1970; Chien & Dickinson, 1972; Yonetani et al., 1974a; Dickinson & Chien, 1980; Hori et al., 1980) in which the only resolved nuclear hyperfine couplings are those from ^{59}Co. The unpaired electron density is associated mainly with the O_2 ligand (Hoffman et al., 1970; Gupta et al., 1975) such that superhyperfine couplings to pyrrole and proximal imidazole ^{14}N nuclei are weak and not resolved.

Weak superhyperfine couplings to ligand ^{14}N nuclei can, however, be resolved by the electron spin echo envelope modulation (ESEEM) technique of pulsed EPR spectroscopy. This method has been used to study electron–nuclear coupling in cupric proteins (Mims & Peisach, 1979; McCracken et al., 1987, 1988), in high- and low-spin ferric hemoproteins (Peisach et al., 1979, 1984; Magliozzo & Peisach, 1992), and in low-spin ferrous nitrosylhemoglobin (Magliozzo et al., 1987), as well as in other paramagnetic biomolecules (Mims & Peisach, 1989). ESEEM spectroscopy of proteins in D_2O provides a rapid and direct method for demonstrating the presence of exchangeable deuterons in the vicinity of the paramagnetic center, such as that in oxyCoMb, and for investigating the magnetic coupling between specific protons/deuterons and the electron spin (Mims et al., 1977, 1984; Peisach et al., 1984; McCracken et al., 1987). One such proton, which participates in a hydrogen bond to the bound O_2 in oxyMb (Phillips & Schoenborn, 1981), has also been suggested to be present in oxyCoMb (Yonetani et al., 1974a; Ikeda-Saito et al., 1977; Petsko et al., 1978; Kitagawa et al., 1982; Walker & Bowen, 1985; Bruha & Kincaid, 1988; Hüttermann & Stabler, 1989). This exchangeable proton and the electron–nuclear interaction for the axial nitrogen are addressed in the present investigation.

† This work was supported by NIH Grants GM-40168 and RR-02583 (to J.P.), GM-39492 and GM-39359 (to M.I-S.), and HL-14508 (to T.Y.).

* Author to whom correspondence should be addressed.
‡ Department of Molecular Pharmacology, Yeshiva University.
§ Case Western Reserve University.
∥ University of Pennsylvania.
⊥ Department of Physiology and Biophysics, Yeshiva University.

[1] Abbreviations: CW, continuous wave; ENDOR, electron nuclear double resonance; EPR, electron paramagnetic resonance; ESEEM, electron spin echo envelope modulation; Hb*gly*, *Glycera dibranchiata* hemoglobin; His-E7, histidine E7, the distal histidine of Mb; His-F8, histidine F8, the proximal histidine of Mb; His-90, the proximal histidine of Hb*gly*; Mb, myoglobin; NMR, nuclear magnetic resonance; NQI, nuclear quadrupole interaction; PAS, principal axis system; PPIX, protophyrin IX; TPP, tetraphenylporphyrin.

[2] E7 and F8 are the alphanumeric codes referring to the position of the residues in the sperm whale Mb amino acid sequence. E7 is the seventh residue in the E helix; F8 is the eighth residue in the F helix (Edmundson, 1965).

0006-2960/92/0431-7274$03.00/0

This paper presents analyses of the ESEEM spectra of the Co(II)-substituted forms of two closely-related hemoproteins, Mb and the monomeric hemoglobin from *Glycera dibranchiata* (Hb*gly*). OxyCoMb has been well characterized by X-ray crystallography (Petsko et al., 1978) and by single-crystal EPR spectroscopy (Chien & Dickinson, 1972; Dickinson & Chien, 1980; Hori et al., 1980). The EPR spectrum of oxyCoHb*gly* in frozen solution has been published (Ikeda-Saito et al., 1977), but no X-ray crystallographic data are available. In their native forms, these two oxygen-carrying hemoproteins have the same prosthetic group and endogenous axial ligand, but differ markedly in their distal environments (Phillips, 1980; Arents & Love, 1989) as well as in their oxygen binding properties (Parkhurst et al., 1980).

Hemoglobin isolated from *G. dibranchiata* contains polymeric and several monomeric forms (Vinogradov et al., 1970; Cooke & Wright, 1985a; Constantinidis et al., 1989). The major monomeric forms exhibit unusually low oxygen affinity (Hoffman & Mangum, 1970; Seamonds & Forster, 1972; Weber et al., 1977), fast oxygen association and dissociation kinetics (Parkhurst et al., 1980), and amino acid compositions which show homology to sperm whale Mb (Imamura et al., 1972; Cooke & Wright, 1985a). The tertiary structure of one of the monomeric forms, as determined by X-ray crystallography, is similar to that of Mb (Padlan & Love, 1974; Arents & Love, 1989). A significant structural difference between Mb and Hb*gly* is the replacement of the distal histidine in Mb by a leucine in Hb*gly* (Cooke & Wright, 1985b; Padlan & Love, 1974; Arents & Love, 1989). Hydrogen bonding to the bound O_2 involving the distal histidine found in Mb (Phillips & Schoenborn, 1981) thus cannot occur in oxyHb*gly*. For this reason, the monomeric Hb*gly* together with Mb, in their Co(II)-substituted forms, provides an excellent system of comparison for the study of the effects of structural differences at the distal side of the prosthetic group on metal–ligand interactions.

Some background for the application of ESEEM spectroscopy to the current investigation comes from ESEEM studies of oxy cobaltous tetraphenylporphyrin (CoTPP) complexes (Magliozzo et al., 1987) in which the coupling to the directly coordinated axial nitrogens and to the pyrrole nitrogens was investigated. Computer simulations of spectra were used to calculate the ligand hyperfine and nuclear quadrupole interaction (NQI) parameters, and a similar approach is used here.

In this paper, the nuclear hyperfine and nuclear quadrupole couplings for the proximal histidyl imidazole N_ϵ in the two Co(II)-substituted proteins are compared. In addition, the hyperfine coupling to an exchangeable deuteron in oxyCoMb, not found in oxyCoHb*gly*, is identified and is ascribed to the deuteron on the distal histidyl imidazole which is hydrogen-bonded to O_2. The role of the hydrogen bonding in modulating the magnetic coupling properties and O_2 affinity of the two oxy cobaltous proteins is discussed using a molecular orbital model for O_2 adducts of cobaltous compounds (Tovrog et al., 1976).

MATERIALS AND METHODS

Protein Preparation. CoMb was prepared as previously described (Yonetani et al., 1974b). Both sperm whale Mb and horse Mb have been used in this study.

G. dibranchiata was purchased from Maine Bait Co., Newcastle, ME. Blood was collected from live worms by incision of the coelomic cavity. Red blood cells were washed four times by centrifugation, using a 1.2% sodium chloride solution. The cells were then resuspended under carbon monoxide and were lysed by two freeze–thaw cycles in liquid nitrogen. The monomer fraction was isolated from the lysate by FPLC on Superose 12 in CO-saturated 0.02 M potassium phosphate buffer, pH 6.8, and was concentrated and oxidized with a 15-fold molar excess of potassium ferricyanide. The oxidized monomers were recovered by FPLC on Superose 12 in 0.02 M potassium phosphate buffer, pH 6.8, concentrated, and used without further purification.

ApoHb*gly* was prepared according to a published procedure (Yonetani, 1967). Cobaltous protoporphyrin IX (CoPPIX) (Porphyrin Products, Logan, Utah) was purified on a silica gel column and reconstituted to apoHb*gly* using the procedure of Yonetani et al. (1974b). The Co(II)-substituted Hb*gly* was charged onto a CM-cellulose column equilibrated with 10 mM phosphate buffer, pH 6. A brown band was eluted, and a red band remained at the top of the column. The brown band was later found to contain EPR-silent material. The column was washed with about 50 mL of 10 mM phosphate buffer, pH 6, and two red bands were eluted with 50 mM phosphate buffer at the same pH. The slower-moving band was used for ESEEM experiments. The ratio of oxy to deoxy protein in this band, measured by optical spectroscopy at room temperature (Yonetani et al., 1974b), was higher than the ratio found for the faster-moving band. This suggests that the slower-moving band contained monomer III according to the nomenclature of Parkhurst et al. (1980), also referred to as monomer A according to the nomenclature of Cooke and Wright (1985a).

Samples of oxyCoHb*gly* were prepared by first transferring the protein into 4-mm EPR tubes which were previously equilibrated with oxygen. The protein was then allowed to equilibrate under an atmosphere of oxygen for 30 min at 0 °C before being frozen. The CW EPR signals (Ikeda-Saito et al., 1977) indicated that the protein was 95% saturated with O_2. The contribution of the 5% deoxy protein to the ESEEM is negligible at $g \approx 2$, the region of major absorption of the oxy protein. Samples of oxyCoMb were frozen in air and were essentially free of deoxy protein. Samples of deoxy proteins were prepared by the addition of a trace amount of dithionite to the oxy protein, followed by equilibration under argon gas at 0 °C for 30 min. EPR and ESEEM samples used generally contained 2 mM protein and 10 mM phosphate buffer in H_2O or D_2O, pH 7. The pH meter readings were not corrected for isotope effect.

Spectroscopy. CW EPR spectra were recorded at 77 K on a Varian E112 spectrometer equipped with a Systron-Donner frequency counter.

ESEEM spectra were recorded at liquid helium temperatures on a pulsed EPR spectrometer previously described (McCracken et al., 1987), using a folded stripline cavity (Britt & Klein, 1987) which can accommodate standard 4-mm EPR tubes. Three pulse, or stimulated echo, experiments (Peisach et al., 1979) were conducted at microwave frequencies between 9 and 11 GHz. The time interval between the first and the second pulses, τ, was chosen to suppress proton modulations (Peisach et al., 1979). Data were collected at the time $2\tau + T$, where T is the time interval between the second and the third pulses. In each individual data set, the time increment of T ranged from 5 to 15 ns. Each data set contained 1024 points, each point representing the average of 20–200 individual measurements of the electron spin echo amplitude. Time domain data were Fourier transformed after dead time reconstruction according to the method of Mims (1984). Quotient spectra for the study of deuterium modulation were obtained by Fourier transforming the ratio of two electron spin echo envelopes for samples in D_2O and in H_2O obtained

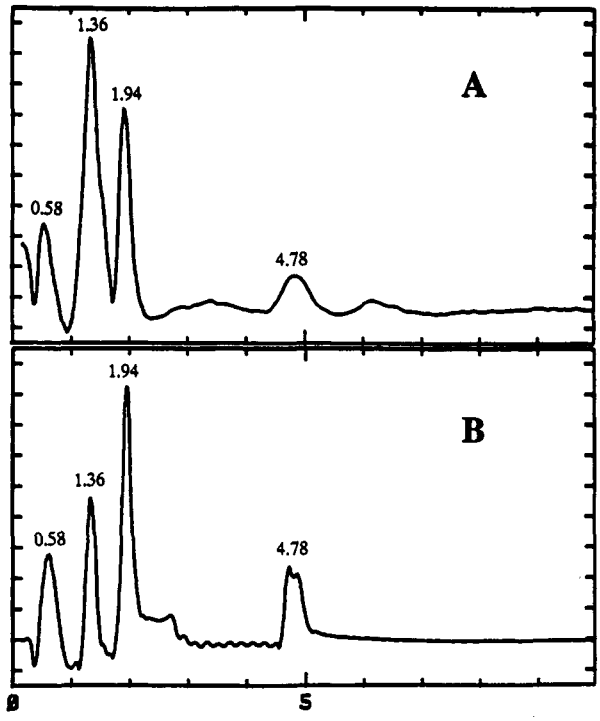

FIGURE 1: (A) ESEEM and (B) computer-simulated spectra of oxyCoMb (horse). Data were collected at microwave frequency = 8.98 GHz, magnetic field = 3149 G (g = 2.038), τ = 149 ns, and temperature = 4.2 K. Parameters used for computer simulation in (B) were A_{iso} = 2.46 MHz, e^2qQ = 2.15 MHz, η = 0.4, r = 3.60 Å, θ = 70°, and β = 90°.

at nearly identical magnetic field and microwave frequency (Mims, 1984). In this way, spectral contributions from identical nuclei in both samples, for example, nonexchangeable protons and ^{14}N, were removed from the data. Spectra interpretation was facilitated by examination of data from experiments at different microwave frequencies and the same experimental g value.

Computer Simulation. Spectral simulation programs used were described previously (Cornelius et al., 1990). The input parameters for a simulation are (i) the principal values of the g and the ^{59}Co ($I = {}^7/_2$) nuclear hyperfine tensors; (ii) the superhyperfine coupling parameters which include coefficients for the nuclear Zeeman, the ligand hyperfine, and the nuclear quadrupole interactions (NQI); and (iii) experimental parameters including the microwave frequency, magnetic field strength, the τ value, and the time increment for data collection. The ligand hyperfine coupling is considered to be axially symmetric and to follow the form of a point dipole model, requiring (i) an isotropic coupling constant, A_{iso}, (ii) an effective dipole–dipole distance, r (Å), and (iii) two angles, θ and ϕ, which describe the relationship between the principal axis system (PAS) of the g tensor and that of the ligand hyperfine tensor. The NQI is characterized by five terms: e^2qQ, the nuclear quadrupole coupling constant; η, the asymmetry parameter; and three Euler angles, α, β, and γ, relating the orientation of the NQI tensor PAS to that of the g tensor. All simulations were performed on a Micro Vax II computer.

RESULTS

OxyCoMb. OxyCoMb exhibits the characteristic four-line ESEEM spectrum (Figure 1A) of a $S = {}^1/_2$ system with weak coupling to ligand ^{14}N nuclei. The spin Hamiltonian for the coupled ^{14}N nucleus contains terms for the ^{14}N nuclear Zeeman, the electron–nuclear hyperfine, and the nuclear quadrupole interactions (Mims & Peisach, 1978). At X-band, in cases where the nuclear Zeeman term is nearly cancelled in one of the electron spin manifolds by the electron–nuclear hyperfine term, the energy level splittings for this electron spin manifold are then mostly determined by the NQI. This condition, sometimes referred to as the condition of "exact cancellation" (Flanagan & Singel, 1987), is evident in oxyCoMb by the appearance of three sharp low-frequency components (0.58, 1.36, 1.94 MHz) where the frequency values of the first two add up to that of the third. The frequencies of these lines show little magnetic field dependence. The fourth line in the spectrum, a broad, higher frequency component, is seen at 4.78 MHz at a magnetic field of 3149 G (Figure 1A). This line shifts to 5.03 MHz at 3525 G. The shift in frequency, 0.25 MHz, is 2 times the increase in Zeeman energy (0.12 MHz), indicating a $\Delta m_I = 2$ transition that arises from the electron spin manifold in which the electron–nuclear hyperfine interaction adds to the nuclear Zeeman interaction (Mims & Peisach, 1978).

The ESEEM spectrum of oxyCoMb is analogous to the spectra of hexacoordinated oxyCoTPP model compounds containing substituted imidazole as an axial ligand (Magliozzo et al., 1987). The study of models containing pyridine or imidazole demonstrated that the spectral components from axial bases arose from the coupling to the directly coordinated ^{14}N. (Poorly-resolved spectral components arising from coupling to pyrrole ^{14}N were also identified.) The ESEEM spectral features of oxyCoMb, however, appear at lower frequencies than those of the model compounds recorded at similar magnetic field settings, suggesting smaller hyperfine and/or nuclear quadrupole coupling to the directly coordinated ^{14}N of the proximal histidyl imidazole (Magliozzo & Peisach, 1992). A computer simulation (discussed in detail below) of the spectrum yielded an isotropic hyperfine coupling (A_{iso}) of 2.46 MHz (Figure 1B). This value is similar to that reported for the directly coordinated axial nitrogen in a 2-methylimidazole oxyCoTPP model (Magliozzo et al., 1987), supporting our assignment of the protein spectrum.

Assignment of the 2.46-MHz coupling to other nitrogen sites, for example, N_δ of the proximal histidine (His-F8), or the pyrrole nitrogens, can be ruled out for the following reasons. We have measured a 1.72-MHz hyperfine coupling to N_δ (His-F8) in deoxyCoMb (data not shown) in which the electron spin is localized primarily on Co (Hoffman et al., 1970). The coupling to this nitrogen in the oxy protein is expected to be smaller as a result of the transfer of an approximate 90% of the spin density from Co to the bound O_2 (Hoffman et al., 1970). Therefore, a value of 2.46 MHz for a nitrogen coupling in oxyCoMb is too large to assign to N_δ (His-F8). The coupling to the pyrrole nitrogens in hexacoordinated oxyCoTPP model compounds is 1.30 MHz (Magliozzo et al., 1987) and would be expected to be similar for the pyrrole nitrogens of the Co-PPIX in oxyCoMb. An A_{iso} of 2.46 MHz is too large for assignment to the coupling to the pyrrole nitrogens. Therefore, the four-line ESEEM spectrum observed for oxyCoMb can reasonably be assigned to the coupling to N_ϵ (His-F8).

The computer simulations used for calculating the coupling parameters for the axial nitrogen require an understanding of the orientation of the g tensor and the Co hyperfine tensor, as well as their principal values in oxyCoMb. This information can be obtained from single-crystal CW EPR studies. However, at cryogenic temperature, the single-crystal EPR spectrum of oxyCoMb (Chien & Dickinson, 1972; Dickinson & Chien, 1980; Hori et al., 1980) shows two species of equal intensity, while only one species is resolved in the EPR spectrum of the protein in solution (Yonetani et al., 1974a). At room temperature, on the other hand, the single-crystal CW EPR

Table I: EPR and ESEEM Parameters of CoMb and CoHb*gly*

protein	EPR $g_\perp$	EPR $g_\parallel$	$A_\perp^{Co}$ (MHz)	$A_\parallel^{Co}$ (MHz)
oxyCoMb[a]	2.080	2.007	46.87	25.44
oxyCoHb*gly*[b]	2.070	2.000	46.64	28.17

protein	field (G)	ESEEM frequencies (MHz)	assignment	A_{iso} (MHz)[c]	e^2qQ (MHz)[c]	η[c]
oxyCoMb	3149	0.58, 1.36, 1.94, 4.78	N_ϵ (His-F8)	2.46	2.15	0.40
oxyCoHb*gly*	3029	1.55, 2.92, 5.85	N_ϵ (His-90)	3.60	2.70	0.50

[a] Yonetani et al., 1974a. [b] Ikeda-Saito et al., 1977. [c] The uncertainties are A_{iso}, ±0.02 MHz; e^2qQ, ±0.02 MHz; and η, ±0.05.

spectrum shows only one signal (Hori et al., 1980), similar to the frozen solution CW EPR spectrum. Therefore, for computer simulation, we used the g tensor and Co nuclear hyperfine tensor axis assignment from the room temperature single-crystal CW EPR study (Hori et al., 1980) such that (i) g_{min} is along the O–O bond and (ii) the angle between g_{min} and A_{min} is 125°, where A_{min} is along the Co–O bond. Furthermore, as a major goal of this work is to compare the superhyperfine coupling parameters of the proximal histidyl N_ϵ nuclei in oxyCoMb and in oxyCoHb*gly*, for which no single-crystal EPR study has been reported, in order to use a consistent approach in both sets of calculations, we have chosen to use the axially symmetric g values and Co hyperfine values ($g_x = g_{max}, g_y = g_z = g_{min}$ and $A_x = A_{max}, A_y = A_z = A_{min}$) estimated from CW EPR studies in solution (Yonetani et al., 1974a; Ikeda-Saito et al., 1977) in the calculation of the coupling parameters for both oxyCoMb and oxyCoHb*gly*, rather than the rhombic parameters from the single-crystal EPR study of oxyCoMb (Hori et al., 1980). Also, the g tensor in oxyCoHb*gly* was assumed to correspond to that in oxyCoMb (Hori et al., 1980). The g and Co hyperfine values used for simulation are summarized in Table I.

The best fit to the ESEEM spectra of oxyCoMb yielded A_{iso} = 2.46 MHz, e^2qQ = 2.15 MHz, and η = 0.40 for N_ϵ (His-F8). Variations of the angles θ, ϕ, α, β, and γ, which describe the relative orientation of the ligand hyperfine, NQI, and g tensors, did not result in much improvement in the match of the intensities of the simulated ESEEM components with those of the data. The simulated spectrum shown in Figure 1B utilized the angles $\theta = 70°$ and $\beta = 90°$, which gave a slightly better fit of the line width of the 0.58-MHz and the 4.78-MHz components as compared to one that assumed an alignment of all three tensors. The Euler angle β corresponds to the angle between the g_{min} axis ($g = 2.007$) and the Q_{zz} axis of the NQI tensor; the latter usually corresponds to the direction of the ^{14}N lone pair donor orbital (Ashby et al., 1978). A large value for this angle is expected as the g_{min} axis is located along the O–O bond (Hori et al., 1980) and the axial nitrogen σ bond is perpendicular to the porphyrin plane.

Previous computer simulations of ^{14}N superhyperfine parameters (McCracken et al., 1989; Cornelius et al., 1990) under conditions of exact cancellation showed that the positions of the three narrow, low-frequency lines are for the most part determined by the values of e^2qQ and η, while their relative intensities are sensitive to the relative orientation of the NQI PAS with respect to the g tensor (i.e., the angles α, β, γ) and the τ value used for the measurement. The position of the broad, high-frequency line is dependent on the ^{14}N nuclear Larmor frequency, the isotropic hyperfine coupling (A_{iso}), and to some extent e^2qQ and η. The line shape of this broad component is sensitive to the nature of the anisotropy of the hyperfine tensor and its orientation with respect to the g tensor (i.e., the angles θ, ϕ). Therefore, simulations that focus on the prediction of the frequencies of the ESEEM components

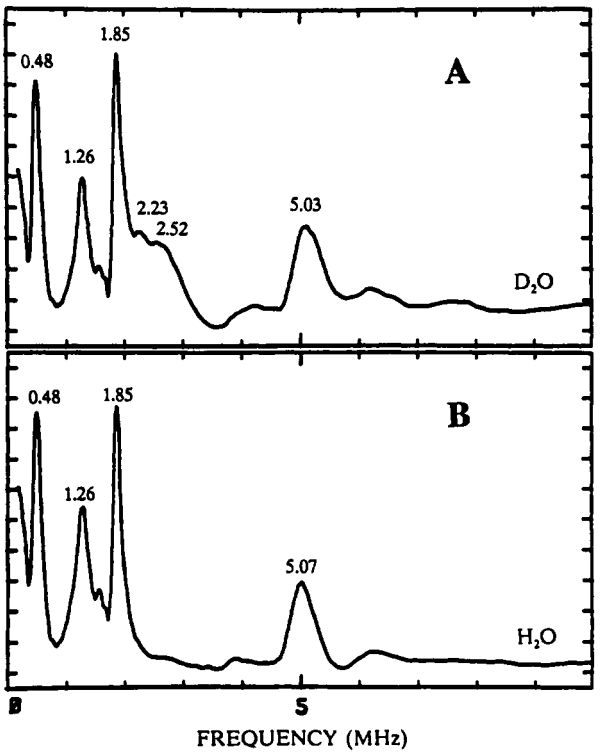

FIGURE 2: ESEEM spectra of oxyCoMb (horse) in (A) deuterated and (B) aqueous buffers. Experimental conditions were (A) frequency = 10.08 GHz, magnetic field = 3535 G (g = 2.038), τ = 199 ns, and temperature = 4.2 K and (B) frequency = 10.06 GHz, magnetic field = 3525 G (g = 2.038), τ = 200 ns, and temperature = 4.2 K.

only, as in this study, are still expected to yield accurate values for A_{iso} and e^2qQ. A possible reason that variation of angles did not give a better fit of the intensities is that the small g anisotropy in the EPR absorption does not allow for a unique orientation selection at a particular magnetic field. Another reason is that the low-frequency spectral lines may contain some contribution from pyrrole nitrogens (Magliozzo et al., 1987).

In order to examine exchangeable hydrogen couplings, the ESEEM spectrum of oxyCoMb in D_2O was investigated and compared to the spectrum of oxyCoMb in H_2O. The ESEEM spectrum of oxyCoMb in D_2O recorded at 3535 G (Figure 2A) shows a low-intensity line at the Larmor frequency of ^2H, and a second line is found 0.3 MHz higher in frequency. In order to visually enhance these new modulation components that arise from ^2H, the electron spin echo envelopes of oxyCoMb in D_2O were divided by that of oxyCoMb in H_2O (Mims et al., 1984). The quotient spectrum obtained by Fourier transforming the ratio of the two electron spin echo envelopes (Figure 3A)[3] shows modulation components at 1.94, 2.24, and 2.53 MHz. This experiment was repeated at another

[3] The quotient spectrum shown is the Fourier transformation of the ratio of two electron spin echo envelopes recorded at a different τ value but at the same magnetic field as the data shown in Figure 2.

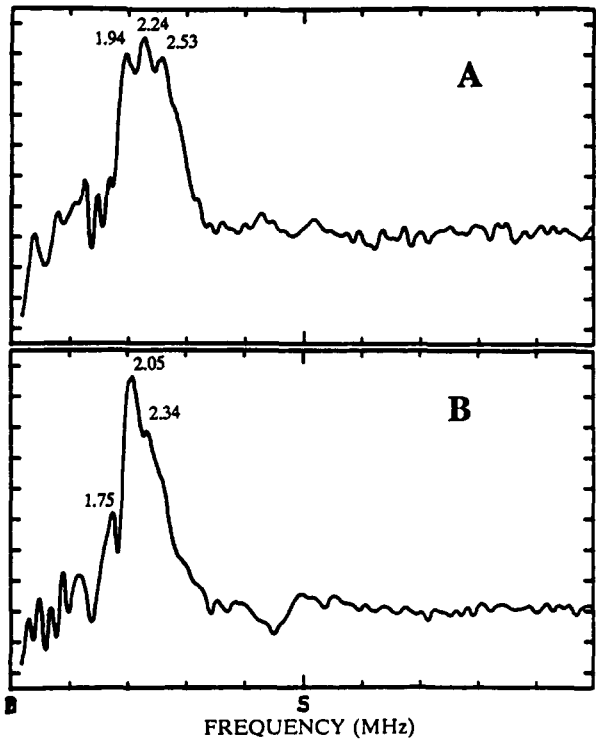

FIGURE 3: Quotient spectra obtained by Fourier transformation of the ratios of the electron spin echo envelopes of oxyCoMb (horse) in D_2O to those of oxyCoMb (horse) in H_2O. Experimental conditions were (A) frequency = 10.06 GHz, magnetic field = 3535 G (g = 2.038), and τ = 133 ns and (B) frequency = 8.98 GHz, magnetic field = 3149 G (g = 2.038), and τ = 149 ns.

magnetic field, 3149 G, and the ESEEM ratio spectrum is shown in Figure 3B. The ^2H modulation components now appear at 1.75, 2.05, and 2.34 MHz. The change in frequency of these three lines corresponds to the shift in Zeeman energy (0.6536 MHz/kG) for ^2H. The central component in both measurements occurs at the ^2H Larmor frequency and is assigned to dipolar-coupled solvent deuterons and other exchangeable deuterons in the vicinity of the paramagnetic center. The remaining two components in both spectra are each offset from the central line by 0.3 MHz and are assigned to deuterium nuclei coupled to the electron spin with a hyperfine coupling coefficient of 0.6 MHz. The frequencies of ^2H ESEEM transitions can be described by

$$\nu(^2H) = \nu(^2H)_{Larmor} \pm {}^1/_2|A_{eff}|$$

with A_{eff} = 0.60 MHz in oxyCoMb. The small quadrupole interaction for ^2H is not expected to be evident in these ESEEM spectra (Mims et al., 1977).

The presence of a sharp ^{14}N component at 1.85 MHz in the data sets used to obtain the ratio spectra presents a complication in the analysis of the ^2H features, since a ^2H component is also expected near this position for a ^2H coupling of 0.6 MHz. In an attempt to resolve the three-line ^2H signal in the Fourier transform spectra, ESEEM spectra of oxyCoMb in D_2O were measured at a microwave frequency of 10.7 GHz (3773 G) (not shown). These measurements, however, did not lead to better resolution of three ^2H lines. A possible reason is the increased contribution of higher order terms to the hyperfine interaction with the increase in magnetic field strength, resulting in a broadening of the frequency components arising from hyperfine interactions. Nevertheless, the two higher frequency lines within the three-line ^2H signal are clearly resolved in ESEEM spectra of D_2O-exchanged samples recorded at 10.08 GHz (3525 G) (Figure 2A) and at 9.46 GHz (3328 G) (data not shown) without resorting to the ratio method, and a coupling to ^2H may still be evaluated on this alone.

The three-line ^2H pattern which scales with magnetic field resembles that seen in the ESEEM spectrum of high-spin met myoglobin in D_2O (Peisach et al., 1984). For that protein, the spectrum showed a line at the Larmor frequency of ^2H together with two flanking components from which a ^2H coupling of 0.8 MHz was calculated. The coupling was assigned to the deuterium of D_2O coordinated to the heme iron.

For oxyCoMb in D_2O, A_{eff} for ^2H coupling measured at three experimental g values (2.09, 2.03, 2.00) is 0.6 MHz. This hyperfine coupling consists of an isotropic contact term and an anisotropic dipolar term. The lack of anisotropy in the measurement might be considered as an indication that the hyperfine coupling is largely determined by a contact interaction. The relative contribution of contact and anisotropic interactions to the total hyperfine coupling was addressed in an ENDOR study of protons coupled to an oxygen radical in irradiated crystalline ribitol (Budzinski et al., 1982). It was found that for a proton 1.79 Å from the radical ≈20% of the effective hyperfine coupling arose from contact interaction. The relative contribution of contact interaction was found to decrease with an increase in the proton–radical distance. The distance between the His-E7 N_ϵ-bound proton, the hydrogen bond donor, and the terminal oxygen in oxyCoMb, is estimated to be 1.39 Å from X-ray crystallographic study (Petsko et al., 1978) of the cobalt protein and a neutron diffraction study of the iron protein (Phillips & Schoenborn, 1981). As the distance between the deuteron and the electron spin on the bound O_2 in oxyCoMb is shorter than the cited proton–oxygen distance in the ribitol radical, the contact contribution is expected to be larger than 20% in oxyCoMb. Our observation of isotropic coupling for the deuterium in oxyCoMb is therefore not inconsistent with a large contact contribution for the hydrogen bond. However, as the g anisotropy in the EPR spectrum of oxyCoMb is small, at any field setting away from the extrema of the spectrum, multiple molecular orientations are selected, and this can prevent the observation of the true anisotropy in the coupling. This apparently isotropic coupling result has a parallel in an ENDOR study of oxy cobaltous hemoglobin A for which a coupling ≈ 6 MHz was found for an exchangeable proton at three experimental g values (Höhn & Hüttermann, 1982).

OxyCoHbgly. The ESEEM spectrum of oxyCoHb*gly* in H_2O (Figure 4A) shows spectral components at 1.55, 2.92, and 5.85 MHz. The spectrum is similar to that of an oxyCo-[^{15}N]TPP–[^{14}N]pyridine model (Magliozzo et al., 1987), suggesting that the protein spectrum contains modulations from the coupling to a directly coordinated axial ^{14}N, the N_ϵ of the proximal histidine (His-90). At higher τ values additional components, believed to arise from the coupling to the pyrrole nitrogens, are resolved at 0.37, 1.17, and 3.90 MHz. These features are not analyzed here.

The ESEEM spectrum of oxyCoHb*gly* was simulated using A_{iso} = 3.60 MHz, e^2qQ = 2.70 MHz, and η = 0.50 (Figure 4C), assuming an alignment of the ^{14}N hyperfine, NQI, and g tensors. The choice of g and Co hyperfine values (Table I) used in the simulation is presented above. Variations of the angles θ, ϕ and the Euler angles α, β, γ had little effect on the simulated spectrum. It should be noted that the hyperfine and quadrupole couplings for the axial nitrogen in oxyCoHb*gly* (Table I) are significantly larger than those for oxyCoMb.

The ESEEM of oxyCoHb*gly* in D_2O (Figure 4B) is unchanged except for some new intensity near 2 MHz. In

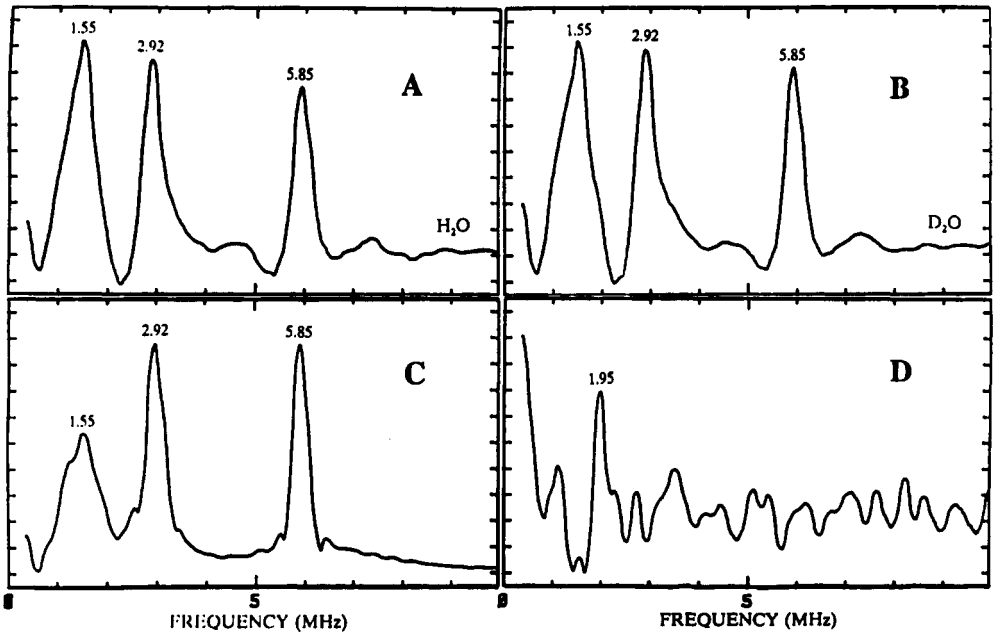

FIGURE 4: ESEEM spectra of oxyCoHb*gly* in (A) aqueous and (B) deuterated buffers. Experimental conditions were (A) frequency = 8.69 GHz, magnetic field = 3057 G (g = 2.03), τ = 154 ns, and temperature = 4.2 K and (B) frequency = 8.69 GHz, magnetic field = 3054 G (g = 2.03), τ = 154 ns, and temperature = 1.8 K. (C) Simulated spectrum of oxyCoHb*gly*. The parameters used were A_{iso} = 3.60 MHz, e^2qQ = 2.15 MHz, η = 0.5, and r = 3.42 Å. (D) Quotient spectrum obtained by Fourier transformation of the ratios of the electron spin echo envelopes of oxyCoHb*gly* in D_2O (B) to that of oxyCoHb*gly* in H_2O (A).

order to enhance the new modulation components, the electron spin-echo envelope of oxyCoHb*gly* in D_2O was divided by that of oxyCoHb*gly* in H_2O as described above. The ratio spectrum is shown in Figure 4D and contains a single component at 1.95 MHz, the ^2H Larmor frequency at 3054 G. This component is believed to arise from weak coupling to deuterons on D_2O or to other exchangeable sites in the vicinity of the paramagnetic center. Ratio spectra obtained at different magnetic field settings also exhibited a single component at the ^2H Larmor frequency. Unlike oxyCoMb, no other components near the Larmor frequency were evident in the ratio spectra.

DISCUSSION

Hydrogen Bonding to the Bound O_2. The presence of a hydrogen bond to the bound O_2 in oxyCoMb is a subject of much interest and has been addressed by X-ray crystallography (Petsko et al., 1978), EPR (Yonetani et al., 1974a; Ikeda-Saito et al., 1977; Walker & Bowen, 1985), resonance Raman (Kitagawa et al., 1982; Bruha & Kincaid, 1988), and ENDOR (Hüttermann & Stabler, 1989) spectroscopy. ESEEM has demonstrated a 0.6-MHz hyperfine coupling of the electron spin in oxyCoMb to an exchangeable deuterium nucleus. This interaction was not seen in oxyCoHb*gly*. The unpaired electron that gives rise to the EPR absorption of oxy cobaltous proteins and compounds has been shown to reside primarily on the bound O_2 (Hoffman et al., 1970; Getz et al., 1975; Gupta et al., 1975; Tovrog et al., 1976; Dedieu et al., 1976). Therefore, the 0.6-MHz coupling seen for oxyCoMb in D_2O demonstrates the presence of a hydrogen near the O_2 ligand, either in a hydrogen bond or covalently attached to oxygen. The latter possibility can be ruled out according to the following argument. The isotropic hyperfine coupling to the proton on a hydroxyl radical is 65 MHz (Box et al., 1970). Assuming 60% spin density on the terminal oxygen in oxyCoMb (Getz et al., 1975; Dickinson & Chien, 1980), the isotropic hyperfine coupling to a covalently bound hydrogen could be as large as 39 MHz, or 6 MHz for the deuteron. As this coupling is 10 times larger than what we observed, a covalent attachment of a deuteron to the bound O_2 is not substantiated.

The observed coupling of 0.6 MHz is also inconsistent with an assignment to the exchangeable deuteron on N_δ (His-F8). The absence of this deuterium coupling in D_2O-exchanged samples of deoxyCoMb (data not shown) and oxyCoHb*gly* substantiates this claim. Since the N_ϵ of His-E7 has been shown to be a hydrogen bond donor site for the terminal oxygen of the bound O_2 in oxyFeMb (Phillips & Schoenborn, 1981), it may be concluded that the coupling of 0.6 MHz arises from the exchangeable deuteron at the same site.

The value of this coupling is 30% smaller than that reported for an exchangeable proton in ENDOR studies of oxyCoHbA (Höhn & Hüttermann, 1982) and oxyCoMb (Hüttermann & Stabler, 1989). The difference in the coupling may be due to structural differences in the protein in D_2O versus H_2O (B. Schoenborn, private communication). These structural differences can lead to small changes in (i) the distance and the relative orientation of the bound oxygen with respect to the coupled proton and (ii) the total unpaired spin density on the O_2 ligand and its relative distribution over the two oxygen atoms. Either or both of these changes may lead to a ^2H hyperfine coupling for the D_2O case that would not be expected to scale to the value measured for a proton in the H_2O case.

Our ESEEM ratio spectra of oxyCoHb*gly* showed a spectral component at the ^2H Larmor frequency only. This component, as well as its counterpart in the ESEEM of oxyCoMb, can only be ascribed to dipolar-coupled exchangeable deuterons on solvent molecules and/or on other exchangeable sites such as amide nitrogens or amino acid side chains. For oxyCoHb*gly*, since there are no ionizable groups on amino acid side chains in the distal pocket (Arents & Love, 1989), the deuterium modulation observed must arise from other exchangeable sites. An additional candidate contributing to this modulation could be the N_δ-bound exchangeable deuteron on the proximal histidyl imidazole which is close enough to the unpaired spin to give a deuterium signal (Mims et al., 1990). The lack of evidence in the ESEEM spectra of oxyCoHb*gly* in D_2O for deuterium coupled more strongly than the population giving rise to a single line at the ^2H Larmor frequency is consistent with the absence of the distal imidazole side chain and the absence of a water molecule on

the distal side (Arents & Love, 1989), hydrogen-bonded to the bound O_2.

Magnetic Coupling and O_2 Affinity of Oxy Cobaltous Globins. The parameters calculated by simulation of ESEEM spectra show weaker hyperfine and quadrupole couplings to the proximal histidyl N_ϵ in oxyCoMb than in oxyCoHb*gly* (Table I). The hyperfine coupling to Co is also slightly smaller in oxyCoMb (Yonetani et al., 1974; Ikeda-Saito et al., 1977). Higher O_2 affinity was found for oxyCoMb than for oxyCoHb*gly* (Ikeda-Saito et al., 1977). These differences between the Co(II)-substituted proteins may be correlated with the known functional and structural differences of the native, iron-containing proteins. For example, Mb has a higher O_2 affinity than Hb*gly* (Parkhurst et al., 1980) and also has a hydrogen bond donor to the bound O_2 not found in Hb*gly* (Phillips & Schoenborn, 1981; Arents & Love, 1989). We would like to propose that this hydrogen bonding accounts for the spectroscopic and functional differences between the two oxy cobaltous forms of these proteins and, in part, for the functional differences between the native proteins.

A molecular orbital model for O_2 adducts of cobaltous compounds (Tovrog et al., 1976) serves here as a means of relating the spectroscopic and functional differences to the relevant bonding orbitals. The σ-bonding molecular orbital, ψ_1, formed upon oxygenation of Co(II) complexes may be considered as a combination of the Co $3d_z2$ atomic orbital with an O_2 π^* molecular orbital together with a small contribution from the cobalt 4s atomic orbital so that

$$\psi_1 = \alpha' 3d_z2 + \gamma 4s + \beta\pi^*$$

The unpaired electron resides in an orbital consisting of the other $O_2\pi^*$ molecular orbital mixed with some Co $d\pi(xz, yz)$ atomic orbitals such that

$$\psi_2 = \beta'\pi^* + \beta'' d\pi(xz, yz)$$

Hyperfine interaction with the Co and axial ^{14}N nuclei results primarily from the interaction of the unpaired spin induced in ψ_1 due to polarization by the unpaired electron in ψ_2 via a spin-exchange mechanism. For Co, the isotropic nuclear hyperfine coupling occurs through the 4s orbital included in ψ_1; and for the axial ^{14}N, the hyperfine interaction occurs primarily through the σ bond between the nitrogen lone pair donor orbital and the Co $3d_z2$ orbital (Wayland & Abd-El-mageed, 1974).

This molecular orbital model helps to illustrate how the Lewis basicity of a nitrogenous axial ligand will modulate the hyperfine coupling to Co and ^{14}N. For example, strong bases, being better lone pair electron donors, will raise the energy of the $3d_z2$ orbital relative to the π^* of O_2. This will decrease the $3d_z2$, and consequently 4s, character in ψ_1, and a smaller hyperfine coupling to Co and axial ^{14}N will result. Decrease in Co (Tovrog et al., 1976) and ^{14}N (Magliozzo et al., 1987) hyperfine interaction with increase in axial base strength has been observed. The quadrupole interaction with the axial ^{14}N is related to the extent of lone pair electron donation from the axial ligand to Co (Hsieh et al., 1977; Ashby et al., 1978). Increase in lone pair donation, for example, in the case of strong axial bases, will reduce the ^{14}N quadrupole interaction. In oxyCoTPP–pyridine model complexes, stronger axial bases were shown to have weaker ^{14}N nuclear quadrupole coupling coefficients (Magliozzo et al., 1987). Additionally, strong bases, by raising the energy of $3d_z2$, will increase the effective π^* character of ψ_1, shifting the electron distribution in the system toward a cobaltic–superoxide configuration (Tovrog et al., 1976). The production of this structure having more π^* character would result in higher affinity for O_2. An increase in O_2 affinity with increase in axial base strength has in fact been observed in a series of CoPPIX complexes (Stynes & Ibers, 1972; Drago et al., 1978).

The above molecular orbital model suggests a correlation between the π^* character in ψ_1 and the magnetic coupling and O_2 binding properties of oxy cobaltous globins. For CoMb and CoHb*gly*, the axial base bound to Co is chemically equivalent and is also considered to be structurally equivalent (see below). We therefore propose that the differences in magnetic coupling and O_2 affinity are a function of a change of the π^* character in ψ_1 due to the hydrogen bonding in oxyCoMb only. As explained above, the π^* character of ψ_1 is related to the cobaltic–superoxide character of the complex (Tovrog et al., 1976), and a hydrogen-bonding interaction to the bound O_2 is expected to electronically stabilize a more ionic species. In this way, the hydrogen bond in oxyCoMb alters the character of ψ_1 in a way similar to increasing axial nitrogen basicity.

Our hypothesis that the spectroscopic changes we observed arose from structural differences in the distal region rather than in the proximal region of the proteins is supported by other spectroscopic studies. The metal–axial imidazole interactions appear to be similar in the deoxy forms of the two ferrous globins. The heme groups have been shown (Takano, 1977; Arents & Love, 1989) to be structurally similar in terms of Fe–N (pyrrole, axial) distances, the dihedral angle between the proximal imidazole plane and the porphyrin N–Fe–N axis, and the orientation of the imidazole plane with respect to the heme normal. Both axial imidazoles are within hydrogen-bonding distance to a backbone carbonyl oxygen. The same resonance Raman iron–histidine stretching mode frequencies were found in the two deoxy globins (Carson et al., 1986). The ESEEM spectra of the two deoxy cobaltous globins are essentially identical (data not shown). Structural similarities in the proximal region of the deoxy proteins need not necessarily be retained in the oxy forms. Nevertheless, similar proximal interactions were also found in the ligated forms of the two ferrous proteins. Upon binding of CO, the NMR chemical shifts of the proximal imidazole protons in Hb*gly* were similar to those of carbonmonoxyMb (Cooke et al., 1987); the similarity was interpreted as hydrogen bonding of the axial imidazole with the protein backbone (Arents & Love, 1989), as in Mb (Hanson & Schoenborn, 1981). An NMR study of the met forms of FeHb*gly* and FeMb (Constantinidis et al., 1988) also suggests that the two proteins have overall similar heme–globin contacts and heme electronic structures.

We therefore conclude that the weaker axial nitrogen superhyperfine coupling in oxyCoMb, compared to that in oxyCoHb*gly*, results from the effects of the hydrogen bond to the O_2 ligand. This hydrogen bond may also stabilize a more cobaltic–superoxide structure and thereby contribute to a higher O_2 affinity in oxyCoMb compared to oxyCoHb*gly*. This same hydrogen bond is likely to contribute to the higher O_2 affinity in native Mb as well.

It should be noted that the differences we observed in hyperfine interaction for the axial ^{14}N in oxyCoHb*gly* could result from an orientation of the bound O_2 in this protein that differs from the geometry in oxyCoMb.[4] The geometric arrangement of the gaseous ligand is expected, in any case, to be related to the features on the distal side, including hydrogen-bonding interactions, so that the issue of ligand orientation is also related to hydrogen bond effects. Without

[4] For CO-bound forms of Mb and Hb*gly*, estimates of Fe–CO bond angles differ by 20° (Padlan & Love, 1974; Hanson & Schoenborn, 1981).

single-crystal EPR measurements and X-ray crystallographic study, these considerations must remain in question.

ACKNOWLEDGMENT

We thank Dr. M. J. Colaneri for helpful discussions. H.C.L. is grateful to F. Jiang for instructions on the operation of the spectrometer and computer simulation programs.

REFERENCES

Arents, G., & Love, W. E. (1989) *J. Mol. Biol. 210*, 149.
Ashby, C. I. H., Cheng, C. P., & Brown, T. L. (1978) *J. Am. Chem. Soc. 100*, 6057.
Box, H. C., Budzinski, E. E., Lilga, K. T., & Freund, H. G. (1970) *J. Chem. Phys. 53*, 1059.
Britt, R. D., & Klein, M. P. (1987) *J. Magn. Reson. 74*, 535.
Bruha, A., & Kincaid, J. R. (1988) *J. Am. Chem. Soc. 110*, 6006.
Budzinski, E. E., Freund, H. G., Potienko, G., & Box, H. C. (1982) *J. Chem. Phys. 77*, 3910.
Carson, S. D., Constantinidis, I., Mintorovitch, J., Satterlee, J. D., & Ondrias, M. R. (1986) *J. Biol. Chem. 261*, 2246.
Chien, J. C. W., Dickinson, L. C. (1972) *Proc. Natl. Acad. Sci. U.S.A. 69*, 2783.
Constantinidis, I., Satterlee, J. D., Pandey, R. K., Leung, H.-K., & Smith, K. M. (1988) *Biochemistry 27*, 3069.
Constantinidis, I., Kandler, R. L., & Satterlee, J. D. (1989) *Comp. Biochem. Physiol. 92B*, 96.
Cooke, R. M., & Wright, P. E. (1985a) *Biochim. Biophys. Acta 832*, 357.
Cooke, R. M., & Wright, P. E. (1985b) *FEBS Lett. 187*, 219.
Cooke, R. M., Dalvit, C., Narula, S. S., & Wright, P. E. (1987) *Eur. J. Biochem. 166*, 399.
Cornelius, J. B., McCracken, J., Clarkson, R. B., Belford, R. L., & Peisach, J. (1990) *J. Phys. Chem. 94*, 6977.
Dedieu, A., Rohmer, M.-M., & Veillard, A. (1976) *J. Am. Chem. Soc. 98*, 5789.
Dickinson, L. C., & Chien, J. C. W. (1980) *Proc. Natl. Acad. Sci. U.S.A. 77*, 1235.
Drago, R. S., Beugelsdijk, T., Beese, J. A., & Cannady, J. P. (1978) *J. Am. Chem. Soc. 100*, 5374.
Edmundson, A. E. (1965) *Nature 205*, 883.
Flanagan, H. L., & Singel, D. J. (1987) *J. Chem. Phys. 87*, 5606.
Getz, D., Melamud, E., Silver, B. L., & Dori, Z. (1975) *J. Am. Chem. Soc. 97*, 3846.
Gupta, R. J., Mildvan, A. S., Yonetani, T., & Srivastava, T. S. (1975) *Biochem. Biophys. Res. Commun. 67*, 1005.
Hanson, J. C., & Schoenborn, B. P. (1981) *J. Mol. Biol. 153*, 117.
Hoffman, B. M., & Petering, D. H. (1970) *Proc. Natl. Acad. Sci. U.S.A. 67*, 637.
Hoffman, B. M., Diemente, D. L., & Basolo, F. (1970) *J. Am. Chem. Soc. 92*, 61.
Hoffman, R. J., & Mangum, C. P. (1970) *Comp. Biochem. Physiol. 36*, 211.
Höhn, M., & Hütterman, J. (1982) *J. Biol. Chem. 257*, 10554.
Hori, H., Ikeda-Saito, M., & Yonetani, T. (1980) *Nature 288*, 501.
Hsieh, Y.-N., Rubenacker, G. V., Cheng, C. P., & Brown, T. L. (1977) *J. Am. Chem. Soc. 99*, 1384.
Hüttermann, J., & Stabler, R. (1989) in *Proceedings of the International Workshop on Electron Magnetic Resonance of Disordered Systems* (Yordanov, N. D., Ed.) p 127, World Scientific Press, Singapore.
Ikeda-Saito, M., Iizuka, T., Yamamoto, H., Kayne, F. J., & Yonetani, T. (1977) *J. Biol. Chem. 252*, 4882.
Imamura, T., Baldwin, T. O., & Riggs, A. (1972) *J. Biol. Chem. 247*, 2785.
Kitagawa, T., Ondrias, M. R., Rousseau, D. L., Ikeda-Saito, M., & Yonetani, T. (1982) *Nature 298*, 896.
Magliozzo, R. S., & Peisach, J. (1992) *Biochemistry 31*, 189.
Magliozzo, R. S., McCracken, J., & Peisach, J. (1987) *Biochemistry 26*, 7923.
McCracken, J., Peisach, J., & Dooley, D. M. (1987) *J. Am. Chem. Soc. 109*, 4064.
McCracken, J., Desai, P. R., Papadopoulos, N. J., Villafranca, J. J., & Peisach, J. (1988) *Biochemistry 27*, 4133.
McCracken, J., Cornelius, J. B., & Peisach, J. (1989) in *Pulsed EPR: A new field of applications* (Keijzers, C. P., Reijerse, E. J., & Schmidt, J., Eds.) p 156, North Holland Publication, Amsterdam.
Mims, M. P., Porras, A. G., Olson, J. S., Noble, R. W., & Peterson, J. A. (1983) *J. Biol. Chem. 258*, 14219.
Mims, W. B. (1984) *J. Magn. Reson. 59*, 291.
Mims, W. B., & Peisach, J. (1978) *J. Chem. Phys. 69*, 4921.
Mims, W. B., & Peisach, J. (1979) *J. Biol. Chem. 254*, 4321.
Mims, W. B., & Peisach, J. (1989) *Advanced EPR Applications in Biology and Biochemistry* (Hoff, A. J., Ed.) p 1, Elsevier Press, Holland.
Mims, W. B., Peisach, J., & Davis, J. L. (1977) *J. Chem. Phys. 66*, 5536.
Mims, W. B., Davis, J. L., & Peisach, J. (1984) *Biophys. J. 45*, 755.
Mims, W. B., Davis, J. L., & Peisach, J. (1990) *J. Magn. Reson. 86*, 273.
Nagai, K., Luisi, B., Shih, D., Miyazaki, G., Imai, K., Poyart, C., De Young, A., Kwiatkowsky, L., Noble, R. W., Lin, S.-H., & Yu, N.-T. (1987) *Nature 329*, 858.
Olson, J. S., Mathews, A. J., Rohlfs, R. J., Springer, B. A., Egeberg, K. D., Sliger, S. G., Tame, J., Renaud, J.-P., & Nagai, K. (1988) *Nature 336*, 265.
Padlan, E. A., & Love, W. E. (1974) *J. Biol. Chem. 249*, 4067.
Parkhurst, L. J., Sima, P., & Goss, D. J. (1980) *Biochemistry 19*, 2688.
Peisach, J., Mims, W. B., & Davis, J. L. (1979) *J. Biol. Chem. 254*, 12379.
Peisach, J., Mims, W. B., & Davis, J. L. (1984) *J. Biol. Chem. 259*, 2704.
Petsko, G. A., Rose, D., Tsernoglou, D., Ikeda-Saito, M., & Yonetani, T. (1978) in *Frontiers of Biological Energetics* (Dutton, P. L., Scarpa, A., & Leigh, J. S., Jr., Eds.) p 1011, Academic Press, New York.
Phillips, S. E. V. (1980) *J. Mol. Biol. 142*, 531.
Phillips, S. E. V., & Schoenborn, B. P. (1981) *Nature 292*, 81.
Seamonds, B., & Forster, R. E. (1972) *Am. J. Physiol. 233*, 734.
Stynes, H. C., & Ibers, J. A. (1972) *J. Am. Chem. Soc. 94*, 1559.
Takano, T. (1977) *J. Mol. Biol. 110*, 569.
Tovrog, B. S., Kitko, D. J., & Drago, R. S. (1976) *J. Am. Chem. Soc. 98*, 5144.
Vinogradov, S. N., Machlik, C. A., & Chao, L. L. (1970) *J. Biol. Chem. 245*, 6533.
Walker, F. A., & Bowen, J. (1985) *J. Am. Chem. Soc. 107*, 7632.
Wayland, B. B., & Abd-Elmageed, M. E. (1974) *J. Am. Chem. Soc. 96*, 4809.
Weber, R. E., Sullivan, B., Bonaventura, J., & Bonaventura, C. (1977) *Comp. Biochem. Physiol. B 58*, 183.
Yonetani, T. (1967) *J. Biol. Chem. 242*, 5008.
Yonetani, T., Yamamoto, H., & Iizuka, T. (1974a) *J. Biol. Chem. 249*, 2168.
Yonetani, T., Yamamoto, H., & Woodrow, G. V., III (1974b) *J. Biol. Chem. 249*, 682.